RSC Advances

PAPER

Cite this: *RSC Adv.*, 2019, **9**, 12310

N-Alkylation *vs.* *O*-alkylation: influence on the performance of the photovoltaic cells based on a tetracyclic lactam polymer donor†

Chenchen Li,[ac] Mian Cai,*[bc] Xichang Bao,[c] Yanfang Liu,[c] Renqiang Yang[c] and Xiaobo Wan*[ac]

Lactam-containing acceptors, which could provide two potential alkylation positions (*N*-alkylation and *O*-alkylation), are important building blocks for polymeric donors in high performance polymer solar cells (PSCs). However, the influence of alkylation positions on the PSC performance has seldom been studied. Herein, we investigated the influence of *O*-alkylation and *N*-alkylation on a novel bislactam acceptor, namely dibenzonaphthyridinedione (**DBND**), on the physical properties of the corresponding polymers and hence their PSC performance. Besides *O*-alkylated and *N*-alkylated DBND, half-*N*-alkylated-half-*O*-alkylated DBND (***N*,*O*-DBND**) was also prepared and copolymerized with stannyl bithiophene (2T). It was found that by varying the alkylation positions, the optical, crystalline and aggregation properties of the corresponding polymers were greatly altered. In comparison with **P(*N*-DBND-2T)** and **P(*O*-DBND-2T)**, **P(*N*,*O*-DBND-2T)** shows both better solubility and shorter $\pi-\pi$ stacking distance. By blending with $PC_{71}BM$, **P(*N*,*O*-DBND-2T)** forms better nano-fibrillar phase separation so that less charge recombination is observed, thus leading to a much better power conversion efficiency (PCE) around 5%, which is the highest value of the conjugated system based on *N*,*O*-alkylated acceptors. The results show that the asymmetric *N*,*O*-alkylation protocol is a promising way to adjust the properties of the bislactam-containing conjugated polymers.

Received 1st March 2019
Accepted 4th April 2019

DOI: 10.1039/c9ra01545k

rsc.li/rsc-advances

Introduction

The past decade has witnessed significant advances in polymer solar cells (PSCs) using donor–acceptor (D–A) type conjugated copolymers as the donor materials in the active layer. Although there are many selectable D building blocks for copolymer construction, the selection pool for A building blocks is relatively limited. Thieno[3,4-*b*]thiophene-2-carboxylate ester,[1–3] benzo-thiadiazole,[4,5] and benzo[1,2-*c*:4,5-*c*′]dithiophene-4,8-dione[6,7] and their derivatives were the few classes of candidates for A units and the polymers based on them exhibited excellent photovoltaic performance. With the development of non-fullerene acceptors, PSCs with a power conversion efficiency (PCE) beyond 13% were reported in recent years.[8–11] Besides these electron-deficient building blocks, another class of potential candidates is lactam-containing aromatics, among which diketopyrrolopyrrolidione (**DPP**)[12–14] and isoindigo(II)[15,16] were well-explored. Polymeric donors based on II and its derivatives exhibiting a PCE beyond 8% in PSCs have been reported.[17,18] The outstanding performance of these bislactam aromatic-based polymers inspires a more extensive study on the synthesis of novel acceptor building blocks containing lactam moieties[19–22] to further adjust the HOMO/LUMO energy level of the corresponding polymers hence the open-circuit voltage (V_{oc}) and current density of the corresponding PSCs devices. For example, Park and co-workers reported the synthesis of 3,7-dithiophen-2-yl-1,5-dialkyl-1,5-naphthyridine-2,6-dione (NTDT), and the polymer based on it exhibited a PCE of 8.16%, which outperformed the similar polymer based on **DPP**.[19] Cao *et al.* synthesized a conjugated polymer based on a bislactam-bridged 1,4-di(thiophen-2-yl)benzene, which showed a high PCE of 7.8% with a high V_{oc} of 0.87 V.[21]

One of the advantages of the lactam-containing acceptors is that the lactam moiety could be very easily alkylated, which endows the corresponding polymers with adjustable solubility and processability. However, an overlooked issue is that there are two positions which could be alkylated on lactam moiety: either the N atom or O atom. In many cases, *N*-alkylated product is the major product since N atom is a softer nucleophile

[a]*Key Laboratory of Optoelectronic Chemical Materials and Devices, Ministry of Education, School of Chemical & Environmental Engineering, Jianghan University, Wuhan 430056, P. R. China. E-mail: wanxb@jhun.edu.cn*

[b]*College of Electronic Engineering and Automation, Shandong University of Science and Technology, 266590 Qingdao, China*

[c]*Qingdao Institute of Bioenergy & Bioprocess Technology, Chinese Academy of Sciences, 189 Songling Road, Qingdao 266101, People's Republic of China. E-mail: caimian@qibebt.ac.cn*

† Electronic supplementary information (ESI) available: Experimental procedures, analytical data, NMR spectra, and crystallographic information (PDF). See DOI: 10.1039/c9ra01545k

compared with O atom. However, when aromatization becomes a driving force, *O*-alkylation overwhelms *N*-alkylation and sometimes only yields *O*-alkylated product. For instance, the alkylation of dihydrodithieno[3,2-*c*:3′,2′-*h*][1,5] naphthyridine-5,10-dione led to a solely *O*-alkylated product, which is an excellent acceptor building block for wide-bandgap (WBG) conjugated polymer.[20] We recently found that a three-step isomerization of II gave a novel bislactam acceptor, dibenzo [*c*,*h*][2,6]-naphthyridine-5,11(6*H*,12*H*)-dione (**DBND**), which is also prone to *O*-alkylation, and the polymer based on it shows a very high PCE (6.32%), although it possesses an ultra-WBG (2.29 eV).[22]

It is very interesting to further probe the influence of *N*-alkylation and *O*-alkylation on the physical property of the acceptor and hence the solar cell performance of the corresponding polymers. Apparently, *N*-alkylation and *O*-alkylation alter the polarity of the corresponding functional group, which may change the π–π interaction distance and strength, UV-vis absorption range and eventually the aggregation state of the corresponding polymers, and all these factors contribute to the final outcome of PSCs performance. However, this topic was seldom touched. Only handful examples were presented in the literature, as summarized in Scheme 1. On one hand, for acceptor containing only one lactam moiety, alkylation may lead to two products: *N*-alkylated product and *O*-alkylated product. The only example we can find is the work from Leclerc's group, in which they compared the PSCs performance of the polymers based on either *N*-alkylated phenanthridin-6-one (***N*-PAD**), or *O*-alkylated phenanthridin-6-one (***O*-PAD**) or a mixture of both acceptors.[23] They found the polymer based on the mixture of both acceptors exhibited the best performance (a PCE of 6.71% with a filled factor (FF) of 67%), and the reason was attributed to the better phase separation of the terpolymer. On the other hand, for bislactam acceptors, the alkylation on the lactam moiety may result in three products: *N*-alkylated product, *O*-alkylated product and *N*,*O*-alkylated product. The first systematic comparison of the alkylation influence on bislactam acceptor, to the best of our knowledge, is the work from Su's group. They synthesized all three alkylated products of pyrido[2,3,4,5-*lmn*]phenanthridine-5,10-dione, namely ***N*-PPD**, ***O*-PPD** and ***N*,*O*-PPD**, and compared the PSCs performance of the polymers based on them.[24] They discovered that the polymer based on ***N*-PPD** showed the best PCE of 3.47%, whereas the polymer based on ***N*,*O*-PPD** showed the worst PCE of 0.46%. They argued that the asymmetric structure of ***N*,*O*-PPD** increased the region-irregularity of the corresponding polymer, which weakened its interaction with PCBM, and led to large phase separation. The alkylation of **DPP** generally leads to *N*-alkylated product, however, *N*,*O*-alkylated product could be obtained in some cases.[25,26] Marks *et al.* compared oligomers based on ***N*-DPP** and ***N*,*O*-DPP**, and they found the oligomer based on the later showed more red-shifted absorption,[23] different from the observation from Leclerc *et al.* that the UV-vis spectrum of polymer based ***N*-PAD** was the most redshifted one.[23] However, the solar cell based on the oligomer of ***N*,*O*-DPP** only exhibited a PCE of 0.56%, much worse than the one based on the oligomer of ***N*-DPP** (PCE 4.02%).[23] More recently, Zhang *et al.* approached the difference of ***N*-DPP** and ***N*,*O*-DPP** at the single molecular level.[24] They found that the conductance of ***N*,*O*-DPP** is more sensitive to acid/base environment change, and one order of magnitude conductance difference was observed. They attributed this to the significant transport path change when ***N*,*O*-DPP** was protonated. We recently synthesized ***N*-DBND** and ***O*-DBND**, and compared the charge transportation behaviors of the polymer based on them. Very interestingly, polymer based ***N*-DBND** showed an almost one hundred times higher charge carrier mobility than the one based on ***O*-DBND**.[27] The much stronger polarity of ***N*-DBND** might be the reason for such a difference.

With the results of different charge transportation behaviors of polymer based on *N*-alkylated and *O*-alkylated DBND in hand, we are eager to see what kind of differences the alkylation position change will bring to the PSCs performance of the corresponding polymers. Here we wish to present a systematic study of the PSCs performance of the polymers based on ***O*-DBND**, ***N*-DBND**, and ***N*,*O*-DBND**. We find that the alkylation position has a strong influence on the UV-vis absorption and also the solubility of the corresponding polymers. When the same long alkyl sidechain is installed, the polymer based on ***N*-DBND** shows the most redshifted absorption but the lowest

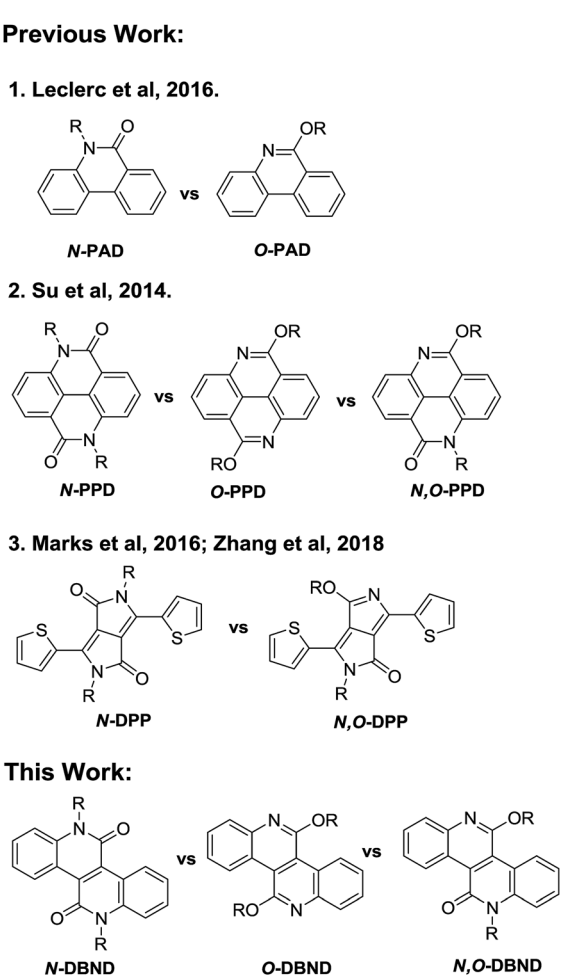

Scheme 1 Study on the influence of *N*-alkylation *vs.* *O*-alkylation of lactam-containing aromatic acceptors on PSCs performance.

solubility, while the polymer based on ***O*-DBND** shows the most blue-shifted absorption but the best solubility. However, both the *N*-alkylated and *O*-alkylated polymers exhibit low PCE (2–3%). On the other hand, the polymer based on asymmetric ***N*,*O*-DBND** shows higher PCE up to 5%, which is among the highest polymer donors with a bandgap around 2.20 eV. This result is very different from the results of Mark's group and Su's group, showing that *N*,*O*-alkylated lactam-containing aromatics can still be a very efficient acceptor building block for WBG conjugated polymers. Grazing incidence X-ray scatting (GIWAXS) and bright field transmission electron microscopy (TEM) techniques and theoretical calculations are used to investigate the corresponding active layer to understand the reason behind it. It is revealed that *N*,*O*-alkylation of **DBND** has two effects: the asymmetric structure not only imposes stronger dipole–dipole interactions on the repeating units, but also the region-irregularity of the corresponding polymer. As the result, polymer based on ***N*,*O*-DBND** exhibits the shortest π–π stacking distance, and the not so-well oriented alkyl sidechain allows the insertion of $PC_{71}BM$ into the polymer matrix to form nanofabric networks with excellent phase separation. This work demonstrates that the semiconducting polymers based on asymmetrically alkylated amide/lactam could also exhibit good PSC performance and molecular design on that kind of structures should not be neglected.

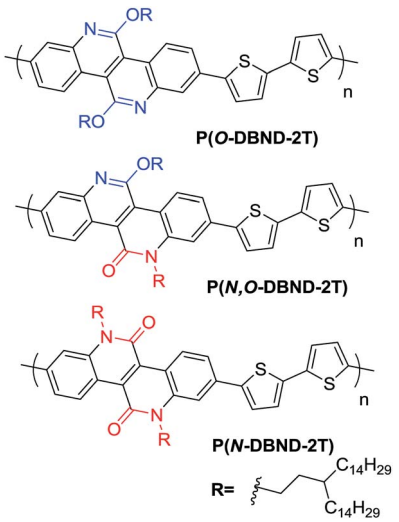

Scheme 2 Structures of P(*O*-DBND-2T), P(*N*,*O*-DBND-2T) and P(*N*-DBND-2T) for PSC study.

Results and discussion

Polymer synthesis and general characterization

The synthesis route towards **DBND** followed our previous strategy,[27] which is also presented in ESI† in detail. It should be mentioned that we have reported that ***O*-DBND** with the branched C24 side-chain (11-methyltricosane) is an excellent building block for WBG conjugated polymers with outstanding performance when copolymerized with 5,5-bis(trimethylstannyl)-2,2-bithiophene (2T).[22] Thus, the corresponding *N*-alkylated and asymmetric *N*,*O*-alkylated DBND with the same C24 side-chain was copolymerized with 2T first to investigate such structure–performance relationship. Unfortunately, unlike the *O*-alkylated polymer, the C24 *N*-alkylated polymer could not be dissolved in chlorobenzene or *o*-dichlorobenzene (*o*-DCB) even when heated up to 140 °C, probably due to the strong intermolecular dipole–dipole interactions between the lactam structures and also the highly planar **DBND** structure.[27,28] Thus, we were unable to fully characterize the properties of the *N*-alkylated polymer on PSCs performance. Therefore, alkylation reagent with longer C31 side-chain (15-(2-iodoethyl) nonacosane) was adopted to improve the solubility, and the newly synthesized monomers were then polymerized with 2T, purified to give the final polymers noted as **P(*N*-DBND-2T)**, **P(*N*,*O*-DBND-2T)** and **P(*O*-DBND-2T)**, respectively, as shown in Scheme 2. With the branched C31 side chain, the solubility of **P(*N*-DBND-2T)** was improved to around 5 mg mL^{-1} in *o*-DCB at 100 °C, which is adequate enough for device fabrication but still not as good as **P(*O*-DBND-2T)** and **P(*N*,*O*-DBND-2T)** (30 mg mL^{-1}). **P(*N*,*O*-DBND-2T)** shows very similar solubility to **P(*O*-DBND-2T)** although it has more polar lactam bonds which generally prefer stronger interchain interaction, and we attribute this to the regio-irregularity it imposed to the polymer which lowers the crystallinity. The molecular weight were determined *via* gel permeation chromatography (GPC) using 1,2,4-trichlorobenzene as the eluent at 150 °C after calibration against polystyrene standards. The average molecular weights (M_n) and polydispersity index (PDI) are shown Table 1. The M_n of **P(*O*-DBND-2T)** and **P(*N*,*O*-DBND-2T)** are 81 kDa and 116 kDa, respectively. However, **P(*N*-DBND-2T)** exhibits a relatively lower M_n (55 kDa) due to its low solubility which hinder the further chain growth during polymerization.

Optical and electrochemical properties

The normalized UV-vis absorption spectra of **P(*O*-DBND-2T)**, **P(*N*,*O*-DBND-2T)** and **P(*N*-DBND-2T)** in diluted *o*-DCB solutions and as thin films are shown in Fig. 1, and the related data are listed in Table 1. The solutions of **P(*O*-DBND-2T)**, **P(*N*,*O*-DBND-2T)** and **P(*N*-DBND-2T)** exhibit absorption in the 400–580 nm region with the maximum absorption peaks at 505 nm, 526 nm and 556 nm, respectively. The red shift of the maximum absorption peaks reflects stronger internal charge transfer effect of D–A structure with the increase of lactam content, which is consistent with the stronger electron-withdrawing ability of the *N*-alkylated lactam moiety than the *O*-alkylated pyridin-2-ol moiety. In the thin film state, **P(*O*-DBND-2T)** and **P(*N*,*O*-DBND-2T)** show similar optical properties to that in solution, whereas **P(*N*-DBND-2T)** exhibits a 5 nm hypsochromic shift when casted into the film, indicating that H-aggregate of **P(*N*-DBND-2T)** is formed in the solid state. No obvious red shift of the absorption onset was observed for three polymers from solution state to solid state. The results indicate that all these polymers might already have adopted a tightly packed aggregation form in solution, which presumably due to the highly planar **DBND** structures that favor better intermolecular interaction.[27,28] The optical bandgaps (E_g^{opt}) of polymers were

Table 1 Molecular weights, optical properties, and electrical properties of DBND based polymers

Polymer	M_n[a] (kDa)	PDI[a]	λ_{max}[b] (nm)	λ_{edge}[b] (nm)	E_g^{opt} (eV)	E_{ox} (V)	IP[c] (eV)
P(*O*-DBND-2T)	81	2.21	505, 472	541	2.29	1.29	5.44
P(*N*,*O*-DBND-2T)	116	1.72	526, 494	563	2.20	1.24	5.39
P(*N*-DBND-2T)	55	2.56	551, 509	575	2.16	1.40	5.55

[a] Determined by GPC at 150 °C using TCB as the eluent. [b] Films are prepared by spin-coated the polymer solution on the piezoid. [c] Films are prepared by dropping-casted the polymer solution on the working electrode.

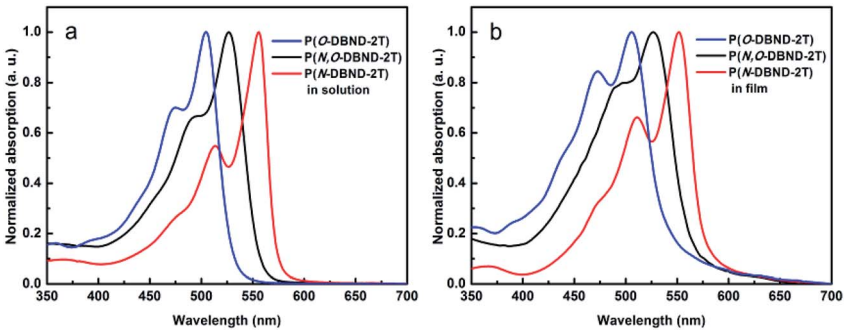

Fig. 1 UV-vis absorption spectra of P(*O*-DBND-2T), P(*N*,*O*-DBND-2T) and P(*N*-DBND-2T) in diluted *o*-DCB (a) and as the thin film (b).

calculated from the absorption edge of the films. The absorption edge is 541 nm for **P(*O*-DBND-2T)**, 563 nm for **P(*N*,*O*-DBND-2T)** and 575 nm for **P(*N*-DBND-2T)** respectively. And the calculated E_g^{opt} are 2.29 eV, 2.20 eV and 2.16 eV, respectively.

Electrochemical cyclic voltammetry (CV) was used to measure the ionization potential (IP) and the electron affinity (EA) of the polymers (Fig. S2†). The IP values (which partially reflects the HOMO energy level[29]) are determined from the onset of the oxidation peak. As is summarized in Table 1, the onset of the oxidation potential of **P(*O*-DBND-2T)**, **P(*N*,*O*-DBND-2T)** and **P(*N*-DBND-2T)** are 1.29 V, 1.24 V and 1.40 V (*vs.* Ag/AgCl), corresponding to a IP value of 5.44 eV, 5.39 eV and 5.55 eV, respectively. The high IP reflects a low lying HOMO energy level, suggesting that the PSCs based on these polymers would exhibit high V_{oc} values. Unfortunately, no well-defined reduction peak was observed, so we could not determine the exact EA of the polymers at this time.

Photovoltaic properties

Solution-processed bulk heterojunction (BHJ) devices based on polymer : $PC_{71}BM$ were fabricated with a conventional device structure of ITO/V_2O_5/polymer : $PC_{71}BM$/Ca/Al. The typical *J*–*V* curves are shown in Fig. 2a and the results are summarized in Table 2. Very interestingly, **P(*N*,*O*-DBND-2T)** exhibits the highest average PCE up to 4.72% (with the highest PCE of 4.96%), which is much larger than that of **P(*O*-DBND-2T)** (2.91%) and almost twice as much as **P(*N*-DBND-2T)** (2.46%). To the best of our knowledge, this result, very different from the results from the previous reports,[23,24] is the first example showing that the performance of the conjugated system based on asymmetrically *N*,*O*-alkylated acceptor unit outperforms the one based on symmetrically *N*-alkylated or *O*-alkylated acceptor units. It is contrary to the generally accepted concept that the more symmetrically alkylated units promote better interchain

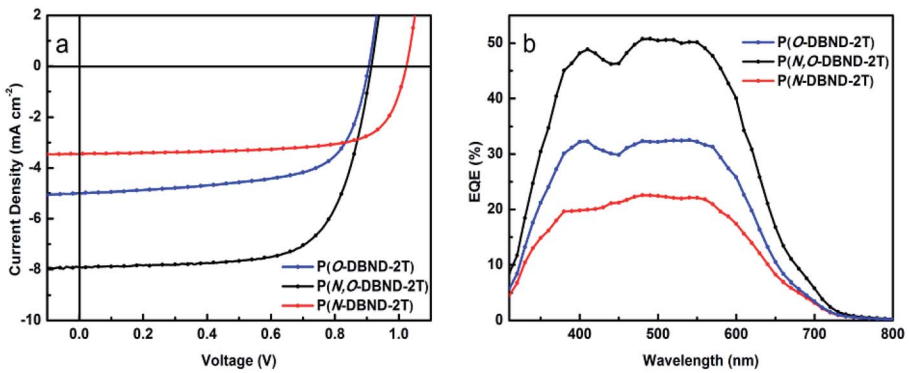

Fig. 2 Photovoltaic characteristics: *J*–*V* curves (a) and EQE (b) plots of polymer : $PC_{71}BM$ (1 : 2 w/w) optimal solar cells under the illumination of AM 1.5 G 100 mW cm^{-2}.

interaction hence better charge transport,[30,31] which is beneficial to the improvement of the organic solar cell performance.[24] However, we also noticed that in recent years, more reports appeared on polymers with asymmetrically alkylated units showing better PCEs that those with symmetrically alkylated units. For example, Shin *et al.* compared the PSCs performance of the polymers containing benzodithiophene (BDT) units with either symmetric alkyl chain or the asymmetric half-alkyl/half-polyethylene glycol sidechain and found that asymmetric one shows higher short circuit current (J_{sc}) and fill factor (FF).[32] Yang *et al.* also discovered that the asymmetric BDT unit substituted by both alkyl/alkoxyl group and aryl group could combine the advantage from two kinds of BDT units and exhibited higher V_{oc} and J_{sc} when copolymerized with a series of acceptor build blocks.[33] The reason why polymer based on ***N*,*O*-DBND** units gives the best PSCs performance deserves further studies and will be discussed in the coming section.

Another feature of the devices based on these three polymers is that regardless of the alkylation types, no additives are needed to adjust their PSCs performance, showing that aggregation behavior of **DBND**-based polymers is mainly governed by their own crystallinity. Also, similar to our previous results, the thicknesses of all the active layers are beyond 250 nm, which is an advantage in fabrication of large area devices since less pinholes and other structural defects present in thicker films.[22] All these features indicate that **DBND** is an acceptor building block for WBG conjugated polymers with excellent processability. On the other hand, the alkylation type does influence the HOMO/LUMO energy level of the corresponding polymers, which is reflected by the V_{oc} change. The V_{oc}s of the devices based on **P(*O*-DBND-2T)** and **P(*N*,*O*-DBND-2T)** are 0.91 V, while that based on **P(*N*-DBND-2T)** is 1.02 V. The larger V_{oc} of device based on the *N*-alkylated polymer is in accordance with its lower HOMO energy level (5.55 eV). *N*-DBND is then one of a few acceptor building blocks the polymer donor based on which could exceed 1.0 V V_{oc} when blended with fullerene acceptors.[34–38] Theoretically, device based on **P(*N*,*O*-DBND-2T)** should exhibit a higher V_{oc} than that based on **P(*O*-DBND-2T)**, however, the same V_{oc} infers that device based on **P(*N*,*O*-DBND-2T)** may suffer from a slight larger voltage loss.

The much better performance of **P(*N*,*O*-DBND-2T)** is attributed to its higher light current. Comparing with the asymmetric polymer **P(*N*,*O*-DBND-2T)** which show a average J_{sc} of 7.48 mA cm^{-2}, symmetric polymers exhibit a rather low J_{sc} (4.62 mA cm^{-2} for **P(*O*-DBND-2T)** and 3.41 mA cm^{-2} for **P(*N*-DBND-2T)**, respectively). In order to confirm the big difference in light current between the symmetric and asymmetric polymers, external quantum efficiency (EQE) of the optical devices are conducted and shown in Fig. 2b. As can be seen from the EQE curves, **P(*N*,*O*-DBND-2T)** blend film shows a response above 40% from 370 to 600 nm, and a strong EQE peak up to 50% in the 475–550 nm regions, which is in consistent of the UV-vis absorption. However the highest EQE peak only reaches to 30% for **P(*O*-DBND-2T)** and 20% for **P(*N*-DBND-2T)**. The calculated EQE matches well with the J_{sc} values with less than 4% mismatch. The hole mobility of **P(*O*-DBND-2T)**, **P(*N*,*O*-DBND-2T)** and **P(*N*-DBND-2T)** are measured and the corresponding results are 1.66×10^{-6} cm^2 V^{-1} s^{-1}, 9.56×10^{-5} cm^2 V^{-1} s^{-1} and 6.18×10^{-6} cm^2 V^{-1} s^{-1}, respectively (Fig. S3†). The **P(*N*,*O*-DBND-2T)** blended film shows a mobility one order higher than that of **P(*O*-DBND-2T)** and **P(*N*-DBND-2T)**, which is also consistent with its higher J_{sc}. To better understand why the *N*,*O*-alkylated polymer performs much better than both *N*- and *O*-alkylated polymers, we set out to study the crystallinity, aggregation state of the polymers and the phase separation behavior of the active layers.

GIWAXS and morphology characterization

The crystallinity and aggregation state of the three polymers are further studied using grazing incidence X-ray scatting (GIWAXS) (Fig. S4†). The out of plane GIWAXS patterns of polymer neat films are present in Fig. 3a. All three polymer films display clear (100), (200), and (300) diffractions at the same position, indicating a similar long-range ordered lamellar packing that rarely affected from the alkylation formation. Obviously, **P(*N*-DBND-2T)** shows a much stronger diffraction at the 2θ value of 2.98° (corresponding to a *d*-spacing of 29.6 Å) than other two polymers, which reflects a much higher degree of crystallinity and is consistent with its low solubility. In addition, strong diffractions around 24.5° indicate a obvious face on molecular orientations exist in the thin films of three polymers. It should be noted that compared with our previously reported *O*-alkylated polymer with C24 side-chain with a π–π stacking distance of 3.74 Å,[22] **P(*O*-DBND-2T)** with C31 sidechain has a shorter π–π stacking distance (3.68 Å). This is in accordance with the well-known conclusion that moving the branch point away from the conjugated backbone favors tighter π–π stacking. Very interestingly, the π–π stacking distance of **P(*N*,*O*-DBND-2T)** is 3.61 Å, much smaller than that of **P(*O*-DBND-2T)**, even smaller than that of **P(*N*-DBND-2T)** (3.63 Å).

To further discuss the difference of aggregation behavior between the **P(*N*,*O*-DBND-2T)** and the other two polymers, density functional theory (DFT) calculation at ωB97XD/6-31G*

Table 2 Average performance parameters of optimal solar cells

Polymer	Film thickness (nm)	μ_h (cm^2 v^{-1} s^{-1})	V_{oc} (V)	J_{sc} (mA cm^{-2})	FF	PCE[a] (%)
P(*O*-DBND-2T)	277 ± 27	1.66×10^{-6}	0.91	5.00 (4.62 ± 0.38)	0.65	2.96 (2.91 ± 0.05)
P(*N*,*O*-DBND-2T)	265 ± 32	9.56×10^{-4}	0.91	7.91 (7.48 ± 0.43)	0.69	4.96 (4.72 ± 0.24)
P(*N*-DBND-2T)	252 ± 15	6.18×10^{-6}	1.02	3.44 (3.41 ± 0.03)	0.71	2.51 (2.46 ± 0.05)

[a] The averages and standard derivations were calculated from at least five devices, optimal polymer : $PC_{71}BM$ ratio is 1 : 2.

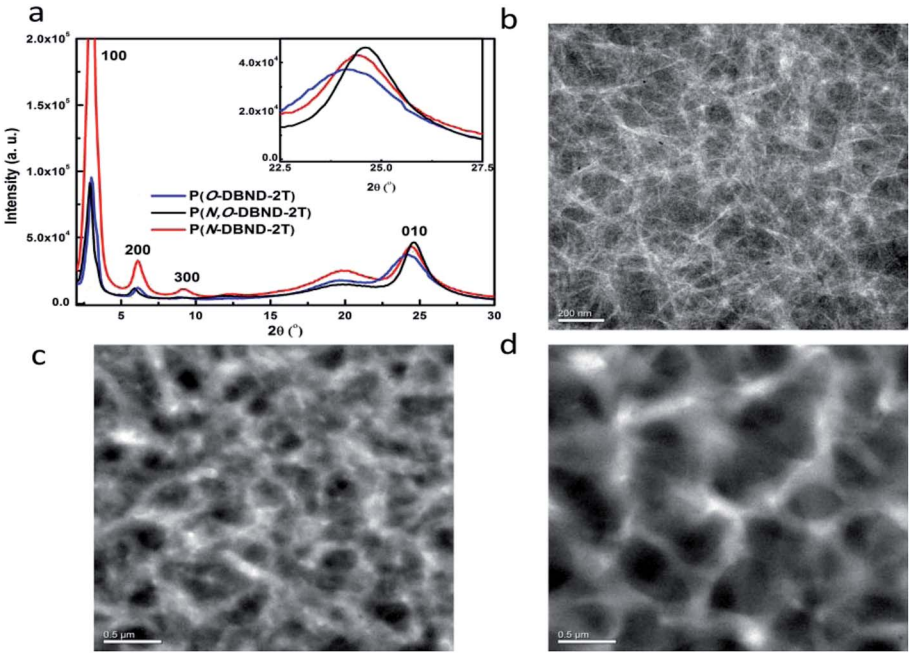

Fig. 3 GIWAXS curves of polymer neat films (a) and TEM images of active layers containing P(*N*,*O*-DBND-2T) : $PC_{71}BM$ (b), P(*O*-DBND-2T) : $PC_{71}BM$ (c) and P(*N*-DBND-2T) : $PC_{71}BM$ (d) in weight ratio of 1 : 2.

level is used to study the energy-minimized structure, dipole moment, as well as the intermolecular self-assembly binding energy (IBE) of *N*,*O*-DBND-2T monomer, and the results are shown in Table 3. To keep consistence with the previous calculation, the 15-ethylnonacosane group (C31 chain) are replaced by 7-ethyltridecane (C15 chain) for *N*,*O*-DBND-2T, same as the calculation structures used for *O*-DBND-2T and *N*-DBND-2T before.[27] Very interestingly, *N*,*O*-DBND-2T exhibits a dipole moment (3.05 D), much higher than that of *N*-DBND-2T (1.56 D) and *O*-DBND-2T (0.49 D). We believe this is caused by the asymmetric structure of *N*,*O*-DBND-2T. The calculated IBE of *N*,*O*-DBND-2T is -61.6 kcal mol^{-1}, which is 4.4 kcal mol^{-1} larger than that of *N*-DBND-2T (-57.2 kcal mol^{-1}), suggesting that **P(*N*,*O*-DBND-2T)** have a stronger intermolecular interaction and greater tendency for stacking. This is consistent with the shortest π–π stacking distance observed for **P(*N*,*O*-DBND-2T)**. Besides this factor, the less steric hindrance caused by the one more atom away branching-point of the alkylated pyridinol moiety might also contribute to the final outcome. However, different from **P(*N*-DBND-2T)** which is highly crystalline and has low solubility due to the strong polar interaction, **P(*N*,*O*-DBND-2T)** has a very high solubility comparable to **P(*O*-DBND-2T)**, and its crystallinity is also similar to **P(*O*-DBND-2T)**. We believe this is due to that *N*,*O*-DBND is region-irregularly incorporated into the copolymers, which lowers the crystallinity of the corresponding polymer and cancels out the possible consequence (lower solubility) caused by higher polarity. The smallest π–π distance of **P(*N*,*O*-DBND-2T)** promotes better Frontier orbital overlap, which is consistent with its highest J_{sc} and highest hole mobility.

Table 3 Calculated dipole moments and intermolecular binding energy for *N*-, *O*-, and *N*,*O*-DBND-2T

	Dipole moment	IBE (kcal mol^{-1})
N,*O*-DBND-2T	3.05 D	−61.6
N-DBND-2T	1.56 D	−57.2
O-DBND-2T	0.49 D	−30.0

The morphologies and phase separation behavior are another key characteristics that determine the J_{sc} values. Bright field transmission electron microscopy (TEM) techniques was employed to cast a light on the difference phase-separation of the active layers formed by the three polymers, and results are shown in Fig. 3b–d. Interestingly, when blended with $PC_{71}BM$, **P(*O*-DBND-2T)** with the bulky C31 side chains exhibits exhibit large polymer domains up to 200 nm, very different from that obtained from **P(*O*-DBND-2T)** with the C24 side-chain, showing that the size of the side-chain has a large influence on the aggregation behavior of **P(*O*-DBND-2T)**. The formation of over-aggregated polymer domains is far beyond the typical exciton diffusion lengths for conjugated polymers (~20 nm)[39,40] This is the reason why **P(*O*-DBND-2T)** with C31 side-chain shows much worse performance than the one with C24 side-chain. Surprisingly, **P(*N*-DBND-2T)** : $PC_{71}BM$ blended film is also composed by large polymer domains up to 200 nm although it shows much worse solubility. On the contrary, **P(*N*,*O*-DBND-2T)** : $PC_{71}BM$ blended film exhibits much smaller polymer domains with less than 40 nm in width and form well-developed nanowire like fibril networks, showing that the aggregation behavior of the polymer based on **DBND** could be finely tuned by choosing the alkylation positions. The well separated nanostructures favors exciton separation and results in much higher J_{sc} and PCE,[41,42] which we believe is benefited from the asymmetric *N*,*O*-alkylated structure. Among all three copolymers. **P(*N*-DBND-2T)** is a symmetric and regioregular D–A type copolymer with polar

lactam moiety, so high crystallinity and strong intermolecular interactions are expected,[30,31] which prevent the insertion of $PC_{71}BM$ into the polymer domains, so large polymeric domains are remained. **P(*O*-DBND-2T)** is also a symmetric and regioregular D–A type copolymer but with less polar pyridinol moiety, so its crystallinity is lower than that of **P(*N*-DBND-2T)**. However, the long C31 sidechain may impose much stronger van der Waals interaction, which may also prohibits the insertion of $PC_{71}BM$ into the polymer domains, so large polymeric domains are still remained, unlike the case when C24 sidechain was used. On the other hand, the crystallinity of **P(*N*,*O*-DBND-2T)** is apparently much lower than that of **P(*N*-DBND-2T)**; which is similar to that of **P(*O*-DBND-2T)**, although the calculated IBE of *N*,*O*-DBND-2T is even higher than *N*-DBND-2T. We postulate that the side-chain of is **P(*N*,*O*-DBND-2T)** not well-orientated due to the region-irregularly incorporated ***N*,*O*-DBND**, which not only decreases the crystallinity of the polymer (but does not change the π–π distance that much), but also provides more room for $PC_{71}BM$ to insert into the polymer matrix. This is the reason why nano-fibril networks of **P(*N*,*O*-DBND-2T)** : $PC_{71}BM$ could still be formed when the rather long C31 sidechain with stronger van der Waals interaction was used.

Conclusions

We have shown here the effect of alkylation positions of the lactam-containing acceptors on the PSCs performance of the corresponding conjugated polymers. And the comparison between the *O*-alkylated, the asymmetric half-*N*-alkylated-half-*O*-alkylated and the *N*-alkylated **DBND** are studied in detail. It was found that with the increased lactam content, the UV-vis absorption of the corresponding polymers red-shifts to longer wavelength, and the polymer based on *N*-alkylated **DBND** exhibits the deepest HOMO energy level of 5.55 eV. It was also found that the alkylation positions have a profound influence on the solubility, crystallinity and aggregation behavior of the polymers. Switching from *O*-alkylation to half-*N*-alkylation-half-*O*-alkylation then to *N*-alkylation, the lactam content of the repeating units increases. However, the increase of lactam content does not lead to the linear increase of the polarity, and theoretical calculation demonstrated that *N*,*O*-DBND-2T exhibits the highest dipole moment due to its asymmetric structure. The highest dipole moment to causes the shortest π–π stacking distance of **P(*N*,*O*-DBND-2T)**, as evidenced by the GIWAXS study. On the other hand, the asymmetric structure of ***N*,*O*-DBND** is a double-blades sword: it also causes the region-irregularity of the corresponding polymers while it strengthens the π–π interaction. As the result, the regio-regular **P(*N*-DBND-2T)** with the medial polarity shows the highest crystallinity. However, due to its high crystalline character, it exhibits the lowest solubility. On the other hand, the regio-regular **P(*O*-DBND-2T)** with the smallest polarity shows the best solubility. Unfortunately, when mixed with $PC_{71}BM$, both polymers show large phase separation domains which is detrimental for PSCs performance, which may be due to that the well-aligned long alkyl chain (C31 chain) of the region-regular **P(*O*-DBND-2T)** and **P(*N*-DBND-2T)** may impose strong hydrophobic–hydrophobic interactions which may not be easily breakdown by $PC_{71}BM$. On the other hand, the region-irregular **P(*N*,*O*-DBND-2T)** with the highest polarity shows very similar crystallinity and solubility to **P(*O*-DBND-2T)**. The region-irregularity allows the relatively easy insertion of $PC_{71}BM$ into the polymer matrix, while the high polarity of the polymer still allows **P(*N*,*O*-DBND-2T)** to form well-developed nanowire like fibril networks. As a consequence, device based **P(*N*,*O*-DBND-2T)** shows a decent PCE around 5%, which is among the best values of WBG polymers with E_g^{opt} around 2.2 eV and the highest value of the conjugated system based on *N*,*O*-alkylated acceptors. Since there is large pool of available conjugated polymers with bis-lactam moiety,[28] our results demonstrated that using asymmetric *N*,*O*-alkylation protocol is a powerful method to finely tune the intermolecular interactions and the phase separation behavior of the corresponding polymers, which is intriguing for side-chain engineering of conjugated polymers.

Experimental

General procedures

All glassware was completely dried before use. Reagents and solvents were purchased from commercial suppliers or purified by standard techniques. Reactions were monitored by thin-layer chromatography by exposing to UV-light irradiation at 254 and 365 nm and/or immersion in a phosphomolybdic acid staining solution followed by drying. Column chromatography was carried out by using silica gel 200–300 mesh. Cyclic voltammetry (CV) curves were measured by dropping cast of polymer film on the working electrode. The measurement were performed on an electrochemistry workstation (CHI660D, Chenhua Shanghai) in anhydrous argon saturated acetonitrile solution (10^{-3} mol L^{-1}) of 0.1 M tetrabutylammoniumhexafluoro-phosphate (*n*-Bu_4NPF_6) at room temperature by three-electrode system, which utilize glassy carbon electrode as the working electrode, Pt as the counter electrode and a Ag/AgCl as the reference electrode at a potential scan rate of 0.1 V s^{-1}. The potential of reference electrode in acetonitrile was identified by using ferrocene as internal standard. The UV-vis spectra were collected with a Hitachi U-4100 UV-vis spectrophotometer in an anhydrous *o*-dichlorobenzene solution (0.01 g L^{-1}) or on a piezoid dropping casted of polymer solution. Gel permeation chromatography (GPC) was performed on Waters 1151 pump and UV-vis monitor (700 nm) using 1,2,4-tricholorobenzene (TCB) as eluent (150 °C). The solution containing polymer and $PC_{71}BM$ was spin-coated onto PEDOT, after PEDOT dissolved in H_2O, the blend film was loaded on copper support film and then sent for bright-field transmission electron microscopy (TEM) characterization after drying. TEM data were acquired using a HITACHI H-7650 electron microscope, and the accelerating voltage is 20 kV. For grazing incidence X-ray scatting (GIWAXS), polymer thin-film samples were illuminated at a constant incidence angle of 0.2° ($\lambda = 2d \sin\theta = 1.54$ Å). The thicknesses of films were determined by XP-2 Profiler (Ambios Technology).

Device fabrication and characterization

Conventional PSCs were fabricated, and the device structures are shown as follows: ITO/V_2O_5/polymer : $PC_{71}BM$/Ca/Al. ITO-

coated glass was ultrasonically washed in detergent, deionized water, acetone, and 2-propanol sequentially for 20 min each. Afterward, the cleaned ITO-coated glass was exposed to oxygen plasma to remove organic contaminants and to increase the size of the wetting envelope. The V_2O_5 layer was prepared through spin-coating a vanadium(v) triisopropoxide oxide alcohol solution (2.5% (v/v)) at 4000 rpm on ITO substrates and then was treated under O_2 plasma for 10 min, without the need for hydrolysis with moisture, or annealed. Subsequently, the modified ITO-coated glass was moved to the glovebox. Polymers and $PC_{71}BM$ were dissolved in *o*-DCB. The solution was stirred overnight at room temperature and then heated for 1 h at 100 °C before being spincoated on V_2O_5 modified ITO-coated glass to form the active layer. The devices were then deposited by Ca (10 nm)/Al (100 nm) as cathode through a shadow mask under high vacuum ($\sim 10^{-4}$ Pa). The thickness of the active layer was controlled by changing the spin speed or solution concentration and was estimated using Veeco Dektak 150 surface profiler. The devices area was 0.1 cm^2 defined by a shadow mask. Current density–voltage (*J–V*) characteristics of the PSCs were recorded using Keithley 2420 source measurement unit under the illumination of AM 1.5 G (100 mW cm^{-2}, Newport solar simulator). Light intensity was calibrated with a standard silicon solar cell. The external quantum efficiencies (EQE) of solar cells were analyzed using a certified Newport incident photon conversion efficiency (IPCE) measurement system. Hole mobility was measured using the space charge limited current (SCLC) model with device configuration of ITO/V_2O_5/polymer : $PC_{71}BM$/MoO_3/Ag by taking current–voltage in the range of 0–5 V and fitting the results to a space charge limited form for a hole-only device. In the presence of carrier traps in the active layer, a trap-filled-limit (TFL) region exists between the ohmic and trap-free SCLC regions. The SCLC behaviour in the trap-free region can be characterized by using the Mott–Gurney equation,

$$J = (9/8)\varepsilon\mu(V^2/L^3)$$

where ε is the static dielectric constant of the medium and μ is the carrier mobility, L is the polymer thickness, and V is the voltage drop across the device. $V = V_{app} - V_{bi} - V_s$, where V_{app} is the voltage applied to the device, and V_{bi} is the built-in voltage resulting from the relative work function difference between the two electrodes, V_s is the voltage drop due to contact resistance and series resistance across the electrodes.

Conflicts of interest

There are no conflicts to declare.

Acknowledgements

We thank the research financial support from National Science Foundation of China (NSFC51573204) and National Science Foundation of Shandong Province (ZR2018ZB0315). X. Bao thanks the Youth Innovation Promotion Association CAS for financial support (2016194). The authors thank Dr Chunming Yang for GIWAXS tests and beamline BL16B1 (Shanghai Synchrotron Radiation Facility) for providing beam time.

Notes and references

1 Y. Liang, D. Feng, Y. Wu, S.-T. Tsai, G. Li, C. Ray and L. Yu, *J. Am. Chem. Soc.*, 2009, **131**, 7792–7799.
2 Y. Liang, Y. Wu, D. Feng, S.-T. Tsai, H.-J. Son, G. Li and L. Yu, *J. Am. Chem. Soc.*, 2009, **131**, 56–57.
3 J. Li, Y. Wang, Z. Liang, N. Wang, J. Tong, C. Yang, X. Bao and Y. Xia, *ACS Appl. Mater. Interfaces*, 2019, **11**, 7022–7029.
4 D. Mühlbacher, M. Scharber, M. Morana, Z. Zhu, D. Waller, R. Gaudiana and C. Brabec, *Adv. Mater.*, 2006, **18**, 2884–2889.
5 K.-H. Ong, S.-L. Lim, H.-S. Tan, H.-K. Wong, J. Li, Z. Ma, L. C. H. Moh, S.-H. Lim, J. C. de Mello and Z.-K. Chen, *Adv. Mater.*, 2011, **23**, 1409–1413.
6 D. Qian, W. Ma, Z. Li, X. Guo, S. Zhang, L. Ye, H. Ade, Z. a. Tan and J. Hou, *J. Am. Chem. Soc.*, 2013, **135**, 8464–8467.
7 D. Meng, D. Sun, C. Zhong, T. Liu, B. Fan, L. Huo, Y. Li, W. Jiang, H. Choi, T. Kim, J. Y. Kim, Y. Sun, Z. Wang and A. J. Heeger, *J. Am. Chem. Soc.*, 2016, **138**, 375–380.
8 J. Wang, J. Zhang, Y. Xiao, T. Xiao, R. Zhu, C. Yan, Y. Fu, G. Lu, X. Lu, S. R. Marder and X. Zhan, *J. Am. Chem. Soc.*, 2018, **140**, 9140–9147.
9 J. S. Zhu, Y. Q. Xiao, J. Y. Wang, K. Liu, H. T. Jiang, Y. Z. Lin, X. H. Lu and X. W. Zhan, *Chem. Mater.*, 2018, **30**, 4150–4156.
10 W. Zhao, S. Li, H. Yao, S. Zhang, Y. Zhang, B. Yang and J. Hou, *J. Am. Chem. Soc.*, 2017, **139**, 7148–7151.
11 S. Li, L. Ye, W. Zhao, H. Yan, B. Yang, D. Liu, W. Li, H. Ade and J. Hou, *J. Am. Chem. Soc.*, 2018, **140**, 7159–7167.
12 P. P. Khlyabich, B. Burkhart, C. F. Ng and B. C. Thompson, *Macromolecules*, 2011, **44**, 5079–5084.
13 W. Li, K. H. Hendriks, A. Furlan, W. S. C. Roelofs, M. M. Wienk and R. A. J. Janssen, *J. Am. Chem. Soc.*, 2013, **135**, 18942–18948.
14 J. Li, Z. Liang, Y. Wang, H. Li, J. Tong, X. Bao and Y. Xia, *J. Mater. Chem. C*, 2018, **6**, 11015–11022.
15 S. Nishinaga, H. Mori and Y. Nishihara, *Macromolecules*, 2015, **48**, 2875–2885.
16 C. Grand, S. Baek, T.-H. Lai, N. Deb, W. Zajaczkowski, R. Stalder, K. Müllen, W. Pisula, D. G. Bucknall, F. So and J. R. Reynolds, *Macromolecules*, 2016, **49**, 4008–4022.
17 L. Zhu, M. Wang, B. Li, C. Jiang and Q. Li, *J. Mater. Chem. A*, 2016, **4**, 16064–16072.
18 W. Yue, R. S. Ashraf, C. B. Nielsen, E. Collado-Fregoso, M. R. Niazi, S. A. Yousaf, M. Kirkus, H.-Y. Chen, A. Amassian, J. R. Durrant and I. McCulloch, *Adv. Mater.*, 2015, **27**, 4702–4707.
19 W. S. Yoon, D. W. Kim, J. M. Park, I. Cho, O. K. Kwon, D. R. Whang, J. H. Kim, J. H. Park and S. Y. Park, *Macromolecules*, 2016, **49**, 8489–8497.
20 R. Kroon, A. Diaz de Zerio Mendaza, S. Himmelberger, J. Bergqvist, O. Backe, G. C. Faria, F. Gao, A. Obaid, W. Zhuang, D. Gedefaw, E. Olsson, O. Inganas, A. Salleo, C. Muller and M. R. Andersson, *J. Am. Chem. Soc.*, 2014, **136**, 11578–11581.

21 J. Cao, Q. Liao, X. Du, J. Chen, Z. Xiao, Q. Zuo and L. Ding, *Energy Environ. Sci.*, 2013, **6**, 3224.
22 M. A. Cai, X. C. Bao, X. Wang, H. R. Zhang, M. Qiu, R. Q. Yang, C. M. Yang and X. B. Wan, *Chem. Mater.*, 2016, **28**, 6196–6206.
23 M. Guérette, A. Najari, J. Maltais, J.-R. Pouliot, S. Dufresne, M. Simoneau, S. Besner, P. Charest and M. Leclerc, *Adv. Energy Mater.*, 2016, **6**, 1502094.
24 M. Liu, Y. Liang, P. Chen, D. Chen, K. Liu, Y. Li, S. Liu, X. Gong, F. Huang, S.-J. Su and Y. Cao, *J. Mater. Chem. A*, 2014, **2**, 321–325.
25 N. Zhou, S. Vegiraju, X. Yu, E. F. Manley, M. R. Butler, M. J. Leonardi, P. Guo, W. Zhao, Y. Hu, K. Prabakaran, R. P. H. Chang, M. A. Ratner, L. X. Chen, A. Facchetti, M.-C. Chen and T. J. Marks, *J. Mater. Chem. C*, 2015, **3**, 8932–8941.
26 Y.-P. Zhang, L.-C. Chen, Z.-Q. Zhang, J.-J. Cao, C. Tang, J. Liu, L.-L. Duan, Y. Huo, X. Shao, W. Hong and H.-L. Zhang, *J. Am. Chem. Soc.*, 2018, **140**, 6531–6535.
27 M. Cai, Z. Y. Zhao, Y. F. Liu, X. Wang, Y. Q. Liu, Z. G. Lan and X. B. Wan, *Macromolecules*, 2017, **50**, 8497–8504.
28 X. Guo, A. Facchetti and T. J. Marks, *Chem. Rev.*, 2014, **114**, 8943–9021.
29 J. L. Bredas, *Mater. Horiz.*, 2014, **1**, 17–19.
30 C. Zhou, G. C. Zhang, C. M. Zhong, X. E. Jia, P. Luo, R. G. Xu, K. Gao, X. F. Jiang, F. Liu, T. P. Russell, F. Huang and Y. Cao, *Adv. Energy Mater.*, 2017, **7**, 1601081.
31 H. Kim, H. Lee, D. Seo, Y. Jeong, K. Cho, J. Lee and Y. Lee, *Chem. Mater.*, 2015, **27**, 3102–3107.
32 Q. V. Hoang, C. E. Song, S.-J. Moon, S. K. Lee, J.-C. Lee, B. J. Kim and W. S. Shin, *Macromolecules*, 2015, **48**, 3918–3927.
33 D. Liu, Q. Zhu, C. Gu, J. Wang, M. Qiu, W. Chen, X. Bao, M. Sun and R. Yang, *Adv. Mater.*, 2016, **28**, 8490–8498.
34 M. A. Faist, T. Kirchartz, W. Gong, R. S. Ashraf, I. McCulloch, J. C. de Mello, N. J. Ekins-Daukes, D. D. C. Bradley and J. Nelson, *J. Am. Chem. Soc.*, 2012, **134**, 685–692.
35 B. Xia, K. Lu, Y. Zhao, J. Zhang, L. Yuan, L. Zhu, Y. Yi and Z. Wei, *Adv. Sci.*, 2015, **2**, 1500021.
36 K. C. Lee, T. Kim, S. Song, Y. Kim, G. K. Dutta, D. S. Kim, J. Y. Kim and C. Yang, *RSC Adv.*, 2016, **6**, 17624–17631.
37 D. Zhu, X. Bao, D. Ouyang, J. Wang, X. Yuan, Q. Wang, D. Zhou, S. Wen and R. Yang, *Nano Energy*, 2017, **40**, 495–503.
38 Z. Ding, X. Long, B. Meng, K. Bai, C. Dou, J. Liu and L. Wang, *Nano Energy*, 2017, **32**, 216–224.
39 A. J. Heeger, *Adv. Mater.*, 2014, **26**, 10–27.
40 M. Drees, H. Hoppe, C. Winder, H. Neugebauer, N. S. Sariciftci, W. Schwinger, F. Schäffler, C. Topf, M. C. Scharber, Z. Zhu and R. Gaudiana, *J. Mater. Chem.*, 2005, **15**, 5158.
41 W. Li, K. H. Hendriks, A. Furlan, W. S. Roelofs, M. M. Wienk and R. A. Janssen, *J. Am. Chem. Soc.*, 2013, **135**, 18942–18948.
42 K. H. Hendriks, G. H. Heintges, V. S. Gevaerts, M. M. Wienk and R. A. Janssen, *Angew. Chem., Int. Ed.*, 2013, **52**, 8341–8344.